Nonlinear Techniques for Forecasting Solar Activity Directly From Its Time Series*

S. Ashrafi and L. Roszman
COMPUTER SCIENCES CORPORATION (CSC)

J. Cooley
GODDARD SPACE FLIGHT CENTER (GSFC)

ABSTRACT

This paper presents numerical techniques for constructing nonlinear predictive models to forecast solar flux directly from its time series. This approach makes it possible to extract dynamical invariants of our system without reference to any underlying solar physics. We consider the dynamical evolution of solar activity in a reconstructed phase space that captures the attractor (strange), give a procedure for constructing a predictor of future solar activity, and discuss extraction of dynamical invariants such as Lyapunov exponents and attractor dimension.

1. INTRODUCTION

1.1 Review of Solar Activity

Need for Solar Flux Prediction. Solar flux $F_{10.7}$ [radio flux emitted at a wavelength of $\lambda = 10.7$ centimeters (cm)] is the best indicator of the strength of ionizing radiations, such as solar ultraviolet and X-ray emissions, that directly affect the atmospheric density and thereby change the orbit lifetime of satellites. Thus, accurate forecasting of solar flux $F_{10.7}$ is crucial for orbit determination of spacecrafts.

Sunspots and Solar Flux. The strong correlation between sunspots and the solar flux $F_{10.7}$ is probably due to the enhanced radiation from limited areas of the Sun where sunspots are active. Sunspot activity depends on the wavelength of radiated solar flux. For waves shorter than 3 cm, the intensity is steady. From 3 to 60 cm, often called the decimeter range, the intensity occasionally increases for a few minutes. Rising from the vicinity of active sunspot regions, decimeter intensity also tends to exhibit a 27-day period associated with solar rotation (Reference 1).

The dynamics of sunspots and their formation are still a mystery. They are often more than 1000 degrees Kelvin cooler than the surrounding photosphere. Although many explanations for sunspot cooling have been proposed (the Biermann field inhibition mechanism and the superadiabatic downflow mechanism), the huge difference in temperature between sunspots and their surroundings suggests a similarity with solitons of multilevel turbulence. One may think of sunspots as solitons in a fluid turbulent Sun (Reference 2). Orbit lifetime is a function of atmospheric drag, which is a function of atmospheric density, which in turn is a function of solar flux. For this reason, spacecraft orbit determination requires accurate forecasting of solar flux.

* This work was supported by the National Aeronautics and Space Administration (NASA)/Goddard Space Flight Center (GSFC), Greenbelt, Maryland, Contract NAS 5-31500.

Nonlinear Structure in Solar Flux. Until recently, we had little reason to doubt that weather is in principle predictable, given enough data. Recently, a striking discovery changed our perspective: simple deterministic systems with only a few degrees of freedom can generate random behavior. When a system exhibits apparent random behavior that is fundamental to its dynamics, such that no amount of information gathering will make the system predictable, the system is considered to be chaotic. Much evidence supports our assertion that solar flux signal falls in this category (References 3 through 11). Perhaps paradoxically, chaos is generated by fixed rules that do not themselves involve any element of chance. Theoretically, the future of a dynamic system is completely determined by present and past conditions. In practice, however, amplification of small initial uncertainties makes a system with short-term predictability unpredictable in the long term.

Many people speak of random processes as though they were a fundamental source of randomness. This idea is misleading. The theory of random processes is an empirical method to deal with incomplete information; it does not attempt to explain randomness. As far as we know, the only truly fundamental source of randomness is the uncertainty principle of quantum mechanics;.everything else is deterministic, at least in principle. Nonetheless, we call many phenomena, such as solar dynamics, random, even though we may not ordinarily think of them in terms of quantum mechanics. Historically, scientists have assumed that randomness derives solely from complication. In this paper, we will take the practical position that randomness occurs to the extent that a system's behavior is unpredictable. We believe that randomness is subjective and a matter of degree; that is, some systems are more predictable than others (e.g., solar activity is more predictable than geomagnetic activity).

Solar Activity Prediction. Interest in solar activity has grown in the past two decades for many reasons. Some reports claim a correlation between solar activity and weather on Earth (Reference 12), although a correlation has not yet been convincingly established (Reference 13). We have some evidence for the coincident occurrences of the Maunder minimum (a period of little or no solar activity occurring from 1645 to 1715) and the "Little Ice Age" (a period of abnormally cold weather) (Reference 14). Perhaps most importantly for flight dynamics, solar activity changes the atmospheric density, which has important implications for spacecraft trajectory and lifetime prediction (Reference 15). The seemingly random nature of solar flux has misled us for many decades, causing us to assume that the underlying physics must necessarily be complex as well. Therefore, researchers have generally used statistical models to predict solar activity (Reference 16). However, new developments in chaos and nonlinear dynamics allow us to model the behavior of a system in terms of some invariants directly extractable from system dynamics, without reference to any underlying physics. Using chaos theory, we can predict short-term activity more accurately than with statistical methods; however, chaos theory imposes a fundamental limit on long-term predictions.

1.2 Brief Review of Chaotic Dynamics

Self-Organization and Attractors. Imagine a very simple system: a pendulum. The pendulum exhibits two fundamental degrees of freedom: position and momentum. However, in its stable periodic state (limit cycle), the pendulum can be described by only one degree of freedom, the phase angle. Here, the dynamic is attracted to a lower-dimensional phase space, and the dimension of this reduced phase space is equal to the number of active degrees of freedom in the self-organized system.

Attractors are not limited to zero dimension (fixed point) or one dimension (limit cycle), but for nonlinear systems they could be high dimensional and in some cases even fractional or fractal (strange attractors).

Nonlinear Dynamical Systems. Anything that moves or evolves in time is a dynamical system. (If it does not move, it is a dynamical system at a fixed point.) Mathematically speaking, a dynamical system can be represented by a state space (phase space) R^M and an evolution operator ψ that defines how the state of the system evolves in time. M is the number of degrees of freedom in the dynamics; ψ can be visualized as the physics of the system.

The attractor A of a dynamical system is the subset of phase space toward which the system evolves:

$$\lim_{t \to \infty} \psi_t(S) = A.$$

An initial condition $\vec{X}_o$ that is sufficiently near the attractor will evolve in time so that $\psi_t(\vec{X}_o)$ gets very close to the set A as $t \to \infty$.

Phase-Space Construction Directly From a Time Series. When confronted with a complicated physical system, an experimenter normally measures at regular and discrete intervals of time the value of some state variable (e.g., flux $F_{10.7}$) and records the time series $f(t_0), f(t_1), f(t_2),...$, with $f(t_i) \in R$ and $t_i=t_0+i\Delta t$. From the observed time series, the experimenter attempts to infer something about the dynamics (i.e., the physics) of the system. The measure f(t) represents a projection π from R^M to R:

$$\pi: R^M \to R.$$

Because the time series is one-dimensional, it is an incomplete description of a system during a time evolution. Nonetheless, many features of the dynamics can still be inferred from the time series alone. From time-delayed values of the scalar time series, Takens (Reference 17) and Packard et al. (Reference 18) have shown that one can embed the time series into a higher dimensional space. Vectors are created with components as

$$\vec{f}(t) = [f(t), f(t-\tau), ... f(t-(m-1)\tau)]^T,$$

where τ (time delay) and m (the embedding dimension) are parameters of the embedding procedure. Here $\vec{f}(t)$ represents a more complete description of dynamics than f(t) and can be thought of as a mapping:

$$\pi^m: R^M \to R^m.$$

An embedding dimension of $m > 2D+1$, where D is the fractal dimension of the attractor, almost always ensures the construction of the topology of the attractor (Takens' theorem, Reference 17).

If unlimited infinitely precise data are available, almost any delay time τ and embedding dimension $m > D$ will work, at least in principle. However, choosing the optimal parameters for real data is a nontrivial process.

For example, if τ is too large then the components f(t) and $f(t+(m-1)\tau)$ of the reconstructed vector $\vec{f}$ will be effectively uncorrelated, which will inflate the estimated dimension. On the other hand, if $(m-1)\tau$ is too small, then the components $f(t),...,f(t+(m-1)\tau)$ will all be very nearly equal, and the reconstructed attractor will look like one long diagonal line. Generally, τ must not be less than some characteristic decorrelation time, and $(m-1)\tau$ must not be much greater than this decorrelation time. One such characteristic time is the local minima of the autocorrelation function $R(\tau) = \langle (f(t)-\langle f \rangle)(f(t+\tau)-\langle f \rangle) \rangle$, where $\langle\ \rangle$ represents average over time.

1.3 Some Invariants of Dynamical Systems

Lyapunov Exponent. In a chaotic system, the adjacent points of the time series become separated under the action of a map; in our case, f_n is the value of solar flux measured daily.

$$f_{n+1} = M(f_n),$$

which leads to satic motion. The Lyapunov exponent $\lambda(\vec{f}_0)$ measures this exponential separation, as shown in Figure 1.

Therefore,

$$\varepsilon_0 e^{N\lambda(f_o)} = |M^N(f_0 + \varepsilon_0) - M^N(f_0)|.$$

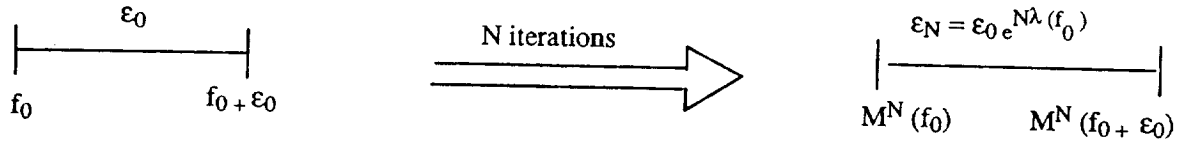

Figure 1. Exponential Separation Measurement

In the limit $\varepsilon_0 \to 0$ and $N \to \infty$, we get the formal expression for Lyapunov exponent $\lambda(f_0)$:

$$\lambda(f_0) = \lim_{N\to\infty} \lim_{\varepsilon_0\to\infty} \frac{1}{N} \ln \left| \frac{M^N(f_0 + \varepsilon_0) - M^N(f_0)}{\varepsilon_0} \right|$$

$$= \lim_{N\to\infty} \frac{1}{N} \ln \left| \frac{dM^N(f_0)}{df_0} \right|.$$

The Lyapunov exponent also measures the average loss of information.

Invariant Measure. The invariant measure $\varrho(f)$ determines the density of the iterates of a map over the unit interval and is defined to be

$$\varrho(f) = \lim_{N\to\infty} \frac{1}{N} \sum_{i=0}^{N} \delta \left[f - M^i(f_0) \right].$$

Kolmogorov Entropy. Kolmogorov entropy K describes the dynamical behavior at the strange attractor. K is the analog of thermodynamic entropy that measures the disorder in a dynamical system. For a one-dimensional map, it is just the Lyapunov exponent. The rate K (at which information about the system is lost) is equal to the average sum of positive Lyapunov exponents:

$$K = \int d^d f \, \varrho(f) \sum_i \lambda_i^+(f),$$

where the superscript d is the dimensionality of our phase space.

In most cases, the λs are independent of f, so

$$K = \sum \lambda_i^+(f).$$

K is, indeed, a useful measure of chaos. K becomes zero for regular motion. It is infinite for totally stochastic or random systems but is a constant larger than zero for chaotic systems (Figure 2). In higher dimensional systems, we lose information about the system (as shown in Figure 3). Here, a sphere of radius ε_0 changes its geometry in phase to an ellipsoid as the system evolves in time.

Hausdorff Dimension. One of the invariants of an attractor that can be extracted directly from the time series is called *Hausdorff Dimension D*, an infinite set of dimensions $D=D_0, D_1, D_2, \ldots$ that describes the inhomogeneity of the attractor. It can be shown that D_2 (which yields a lower bound on the Hausdorff dimension) and many other invariants of the system can be directly obtained from a time series:

- D_2, that is, a lower bound on the Hausdorff dimension ($D_2 < D_1$)
- d, that is, the embedding dimension of the attractor
- The amplitude of the white noise on the signal; that is, separating the deterministic chaotic motion of the system from disturbing white noise

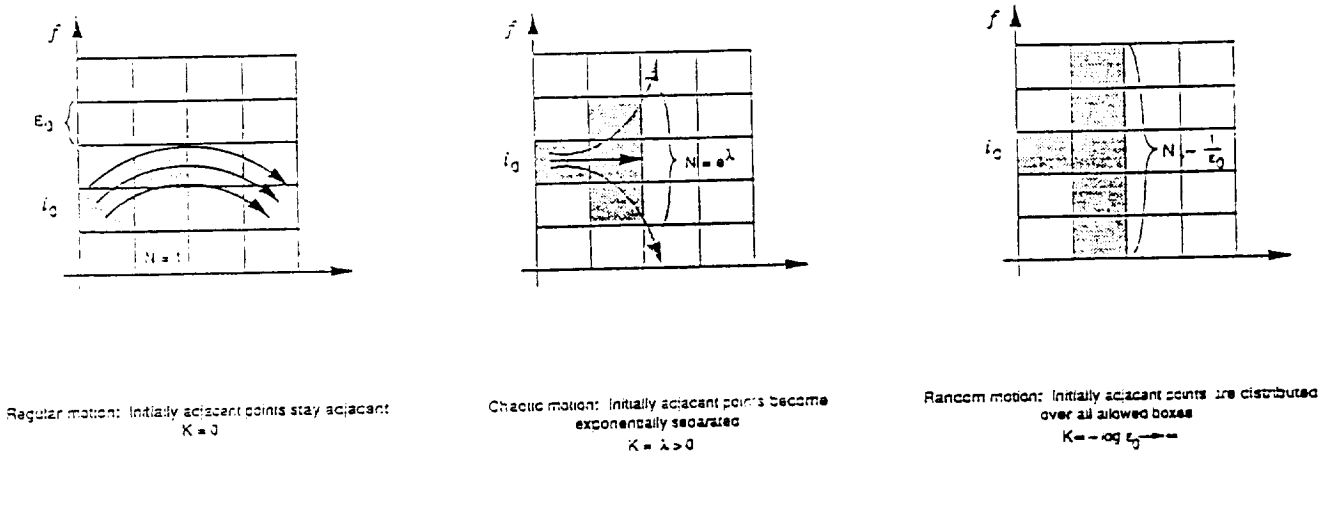

Figure 2. Kolmogorov Entropies for Regular, Chaotic, and Random Motions

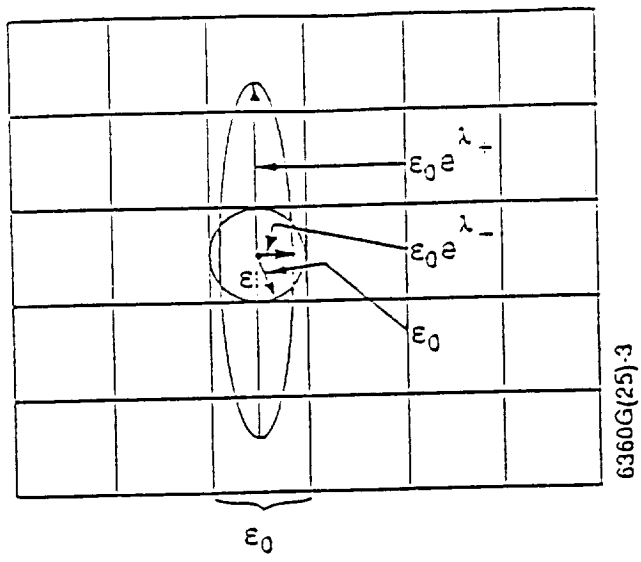

Figure 3. A Two-Dimensional Map of Small Circle Into an Ellipse

- A lower bound on the Kolmogorov entropy; that is, determining "how chaotic" the signal is
- The Kaplan-Yorke dimension: connects the static structure of the attractor (as measured by $D=D_0, D_1, D_2, \ldots$) and the dynamical behavior at the attractor (as measured by the Lyapunov exponents)

Dimensions of a Strange Attractor. To characterize the inhomogeneous static structure of the attractor, we introduce an infinite set of dimensions D_n related to the nth powers of P_i via

$$D_n = \lim_{\varepsilon_0 \to 0} \frac{1}{n-1} \frac{\log \left[\sum_{i=0}^{Q(\varepsilon_0)} P_i^n \right]}{\log \varepsilon_0}$$

$$n = 0, 1, 2, \ldots,$$

where P_i is the probability of finding a point of attractor in the cell number i [i=1, 2, ... Q (ε_0)]. For n=0, we get the Hausdorff dimension of the attractor $D=D_0$; for n=1, we get dimension $D=D_1$ (called the *information dimension*). It should be noted that for $n \to \infty$, the dimension is still a finite number (D_∞=finite), which in general is not an integer.

Largest Lyapunov Exponent of Solar Flux Time Series. The sum of the Lyapunov exponents is the time-averaged divergence of the phase space trajectory; hence, any dissipative dynamical system will have at least one negative exponent. Any dynamical system without a fixed point will have at least one zero Lyapunov exponent.

A small positive Lyapunov exponent is an indication of chaos, and a very large positive Lyapunov exponent is an indication of a totally stochastic or random system. Therefore, the sign of the exponent provides a qualitative picture of a system's dynamics—a positive exponent represents chaos, a zero exponent represents marginally stable systems, and a negative exponent represents periodic systems. Figures 4 and 5 show the actual solar flux data and the largest Lyapunov exponent, respectively, for more than 4000 points. Here, we have used the well known technique of phase space reconstruction with delay coordinates (Reference 18). After embedding the solar flux time series in a state space using the Takens-Packard delay coordinate technique, one can "learn" the induced nonlinear mapping using a local approximation. This will allow us to make short-term forecasting of the future behavior of our time series using information based only on past values. The error estimate of such a technique has already been developed by Farmer and Sidorowich (Reference 19).

$$E \approx C e^{(m+1)KT} N^{-(m+1)/D},$$

where
- E = normalized error of prediction ($0 \leq E \leq 1$, where zero is perfect prediction and one is a prediction no better than average)
- m = order of local approximation
- K = Kolmogorov entropy
- T = forecasting window
- N = number of data points
- D = dimension of the attractor
- C = normalization constant

Using the Farmer-Sidorowich relation, we can find the prediction horizon T for the zeroth order of local approximation. Any prediction above T_{max} is no better than average constant prediction.

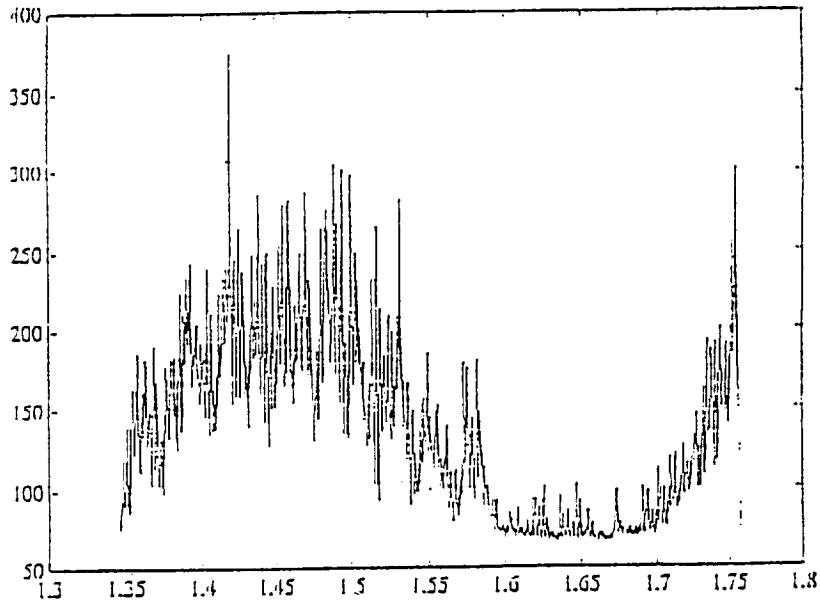

Figure 4. Actual Solar Flux Time Series

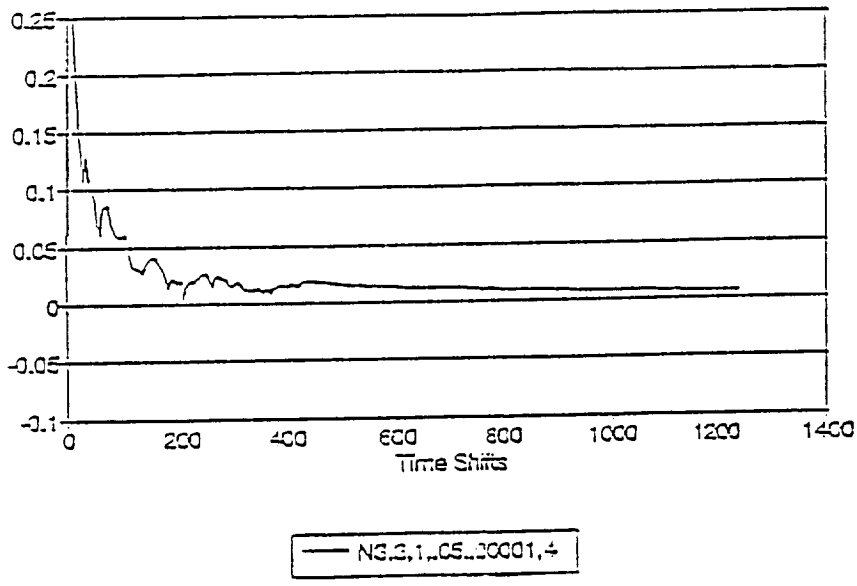

Figure 5. Largest Lyapunov Exponent of Solar Flux Time Series of Figure 4

$$E(T_{max}) = 1$$

Thus, for m = 0, K is the largest Lyapunov exponent λ. Therefore,

$$e^{KT_{max}} N^{-1/D} \sim 1 \qquad \text{or} \qquad T_{max} \sim \frac{\ln (N)}{KD}$$

$$T_{max} \sim \frac{\ln (N)}{\lambda D}$$

Any prediction beyond the indicated horizons is no better than average value. The connection between the local and the global Lyapunov exponents has recently been found (March 1991) by Abarbanel et al. (Reference 20) in a form of power law as

$$\lambda(l) = \lambda_G + \frac{c}{l^\nu}$$

$$N = \omega l,$$

where $\lambda(l)$ = local Lyapunov exponent
l = length of observed data (observation window)
ν = a constant dependent to the dynamical system ($0.5 \leq \nu \leq 1.0$)
c = a constant dependent to initial conditions of the system
λ_G = well known global Lyapunov exponent
ω = frequency of data points

Because any data are finite length data, using the Abarbanel-Kennel power law and Farmer-Sidorowich relation, we can find T_{max} as

$$T_{max} \sim \frac{\ln(l\omega)}{\left(\lambda_G + \frac{c}{l^\nu}\right) D} .$$

This means that as l increases linearly, T_{max} increases logarithmically to a certain asymptotic T because of the denominator c/l^ν (Figure 6).

Therefore, our relation shows that at the asymptote $T_{max} = T_0$ (Reference 11) and $dT_{max}/dl = 0$. Thus, we can find what observation window is required for forecasting up to T_{max} within some confidence level.

$$\frac{dT_{max}}{dN} \rightarrow 0, \text{ thus } N_0 \sim e^{\frac{x_0(\delta)}{\nu}}, \; x_0(\delta) > 2,$$

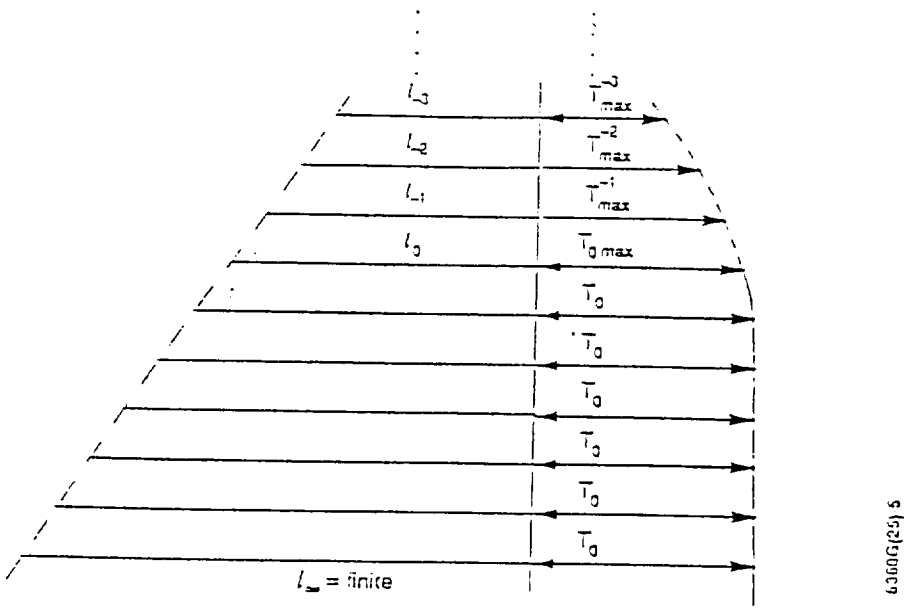

Figure 6. Relationship of l to T_{max}

where $x_0(\delta)$ is the solution to $e^{-x}(x - 1) = \delta$, and where

$$\delta = \frac{\lambda_G}{c\omega^v}$$

is the scaled global Lyapunov exponent.

This result shows that any observation window greater than $l_0 = N_0/\omega$ will not improve our prediction horizon T_0; so more data beyond this limit are not needed to understand a dynamical system. This conclusion is indeed consistent with weather prediction and also with empirical results concluded from neural networks training.

2. STRUCTURE OF THE COMPUTER PROGRAM

Once we know the state space representation, the next goal is to fit a model to the data. There are several methods. The simplest method is to assume that the dynamics can be written as a map in the form

$$f_{n+1} = M(f_n),$$

where the current state is f_n, and f_{n+1} is a future state. Methods such as the polynomial method, rational approximation, radial basis functions, neural networks, and local approximations have been proved to be successful. Here we only introduce local approximation technique, which is the method used to structure the computer program.

Local Approximation. The basic idea is to break up the domain of M into local neighborhoods and fit different parameters into each neighborhood. This fit is generally better than global approximation, especially for large data sets. Most global representations reach a point of diminishing returns, at which adding more parameters or data gives only an incremental improvement in accuracy. After a certain point, adding more local neighborhoods is usually more efficient than adding more parameters and going to higher order. With local approximation, it is possible to use a given functional representation efficiently. The key is to choose the local neighborhood size correctly, so that each neighborhood has just enough points to make the local parameter fits stable. The basic idea is shown in Figure 7 .

Moving to representations of higher degree involves a tradeoff—higher degree representations promise more accuracy, but also require larger neighborhoods. A larger neighborhood implies that the complexity of M increases. Finding the best compromise between these two effects is a central issue in local approximation.

An example of local approximation is *first order*, or *nearest neighbor*, approximation. Look through the data set for nearest neighbor, and predict the current state based on what the neighbor did at time T later. We approximate $f(t + T)$ by $\hat{f}(t, T) = f(t' + T)$, where $f(t')$, is the nearest neighbor of $f(t)$. That is, to predict tomorrow's solar flux, we would search the historical record and find the solar flux pattern most similar to that of today, and predict that tomorrow's solar flux pattern will be the same as the neighboring pattern 1 day later.

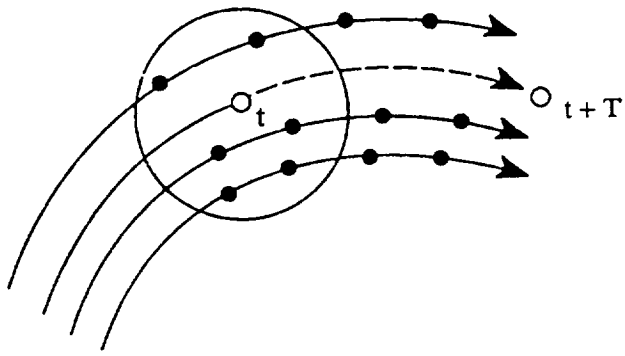

Figure 7. Phase Space Trajectories

First order approximation can sometimes be improved by finding more neighbors and merging their predictions, for example, by weighting according to distance from the current state. If the data are noise, it is better to use a larger number of neighbors. This procedure can be improved by weighting the contributions of neighbors according to their distance from the current state. The beauty of linear approximation is that the neighborhood size grows slowly with the embedding dimension. The order of approximation may depend on factors such as the choice of neighborhoods, the dimension, or peculiarities of the data set. For low dimensional problems, a third order approximation is good.

Nonstationary Behavior. If the trajectory is on an attractor, the data must be stationary, as long as the parameters are constant. However, parameter variations can result in nonstationary behavior. To deal with this problem, we include time as one of the state space coordinates. Time can be included in the metric, so that the search for nearest neighbors favors recent data. This approach takes into account the trends, other time-dependent effects, and seasonality.

Implementation of Local Approximation. Finding neighbors in a multidimensional data set is time consuming when considering many points. A straightforward method is to compute the distance to each point, which takes approximately N steps for N points. This can be reduced to roughly log N steps by organizing the data with a decision tree, such as a k–d tree (Reference 21).

In this method, the data set is partitioned one coordinate at a time. We can take the coordinate with largest range and partition it at its median value. These values are stored in the tree as *keys*. It is now possible to eliminate many points form consideration when looking for the nearest neighbors. This way, we minimize processing time considerably.

2.1 CHOICE OF THE EMBEDDING DIMENSION d

Here we would like to determine the correct value of the embedding dimension d from the scalar time series $x(n)$, $n=1,2,...,N_D$. We assume that there are enough data that we need not be concerned with statistical issues about numerical accuracy. We also assume that extrinsic noise is absent from the $x(n)$ when we receive them. We further assume that by following Takens' phase-space reconstruction technique we have successfully captured the dynamics and embedded our time series. This requires a correct choice of τ, which will be discussed in the next section.

For now, let's further assume we have a correct τ to construct the attractor in the phase space. To establish dimension d, we need some characteristic of the attractor that becomes unchanging as d becomes large enough, thus indicating that the attractor can be embedded in R^d. This invariant characteristic of the attractor is the attractor dimension d_A. One increases d until d_A remains constant and identifies the minimum d where d_A "saturates" as the embedding dimension. But computation of d_A is difficult, so we use the correlation function D(r) proposed by Takens (Reference 17).

$$D(r,N,d) = \frac{2}{N(N-1)} \sum_{i=1}^{N} \sum_{j=i}^{N} U(r - \| \vec{f}(j) - \vec{f}(i) \|) \quad i \neq j,$$

where U(z) is just the unit step function $U(z) = \begin{cases} 1 & z>0 \\ 0 & z<0 \end{cases}$.

For N large enough, the behavior of D(r,N,d) for r becomes independent of N and D(r,N,d) takes the form

$$D(r,N,d) = \Phi(r,d) r^{\nu(d)}.$$

If we plot D(r,N,d) versus r we can single out the correct value of dimension d as in Figure 8. From Figure 8 it is concluded that the minimum value of d=3 is the right choice beyond which attractor dimension d_A does not change or the slope of our graph becomes constant.

In the next section we study the correct choice of τ to reconstruct the phase-space attractor.

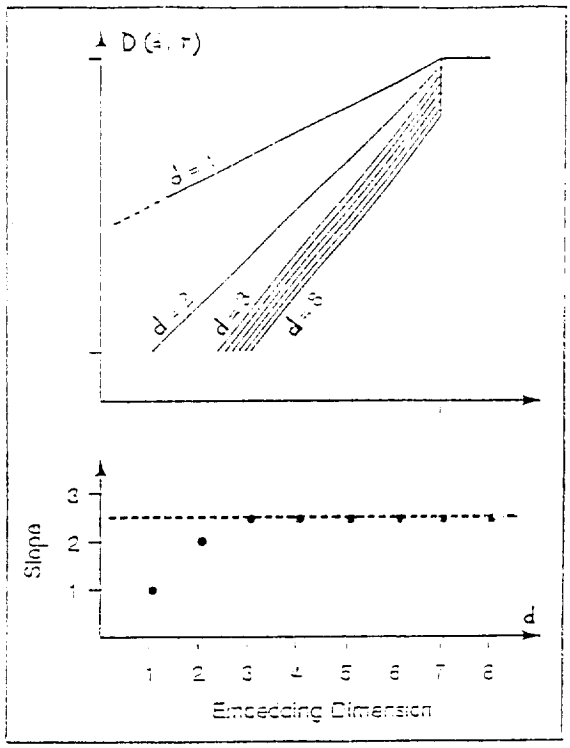

Figure 8. Correlation and Attractor Dimensions

2.2 Choice of the Time Shift τ

The choice of time shifts τ is not well agreed upon. If the underlying system is described by a differential equation and scalar variable x(t) were measured at discrete times $x(n) = x(t_o + n\,\Delta t)$, then we would be, by the choice of lagged variables, trying to find a discrete replacement for the usual phase-space coordinates:

$$x(t), \dot{x}(t), \ \ddot{x}(t), \ldots \frac{d^{d-1}x(t)}{dt^{d-1}}.$$

The best choice for time shift τ is a fraction of the time associated with the first local minimum of the autocorrelation function

$$\frac{1}{T}\int x(t+\tau)x(t)dt\,.$$

We find that this choice, although somewhat arbitrary, works well in practice and gives a simple systematic way of determining τ.

3. RESULTS

Figure 9 shows the daily observed values of solar flux $F_{10.7}$ for about four solar cycles from February 1947 to November 1991. A close examination of this graph shows low daily variability at solar cycle minima and large daily variability at solar cycle maxima. Therefore, the challenge for solar physicists is to forecast solar flux in the region of solar cycle maxima.

Here forecasts are made in the region of solar cycle maxima, where the variations are as large as 150 units of solar flux, and in regions between a maximum and a minimum, where the variations are as large as 100 units of solar flux. Comparisons are made versus 27-day NOAA predictions, Schatten's monthly predictions, and

observed values of flux $F_{10.7}$. Figure 10 shows 27-day predictions using chaos theory with undecoupled (raw) data. Predictions were made in the region of solar cycle maxima. Comparisons show clearly that chaos predictions are at worst 20 units off from observed values, whereas the best NOAA 27-day predictions are about 40 units off from observed values, with a wrong phase on the 27-day local maximum.

Here it is clear that chaotic long-term prediction is very close to the 81-day average of actual $F_{10.7}$, which is useful for calculating exospheric temperature using the Jacchia-Roberts atmospheric density model.

Figure 11 shows the same conclusion for predictions made for a 60-day span. Here it is very clear that NOAA predictions (best updated values to the end of 60 days) do not carry any of the significant dynamical features of the observed values, whereas the chaos prediction does carry the inherent dynamical features. Figure 12 shows a comparison of MSFC and Schatten's predictions. Figure 13 also shows comparisons of 81-day average $F_{10.7}$, Schatten's predictions, and chaos predictions.

Figure 14, which was made for a region between solar cycle maxima and minima, shows a 30-day prediction indicating that chaos prediction is at worst 20 units off from the observed values, but it should be noted that the signal-to-noise ratio characteristic of solar activity indicators are ~ 35 for $F_{10.7}$, ~ 20 for sunspot numbers, and ~ 10 for sunspot areas.

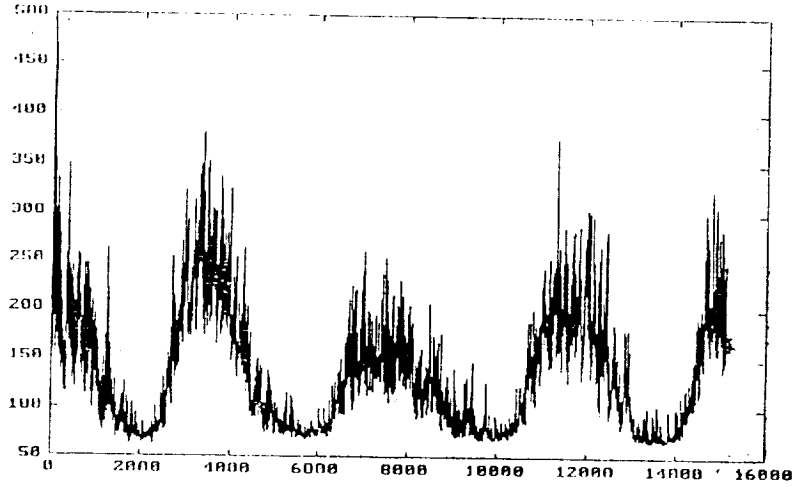

Figure 9. Daily Observed Values of Solar Flux $F_{10.7}$ (Watt per m^2 per Hz x 10^{-22}) Versus Modified Julian Date

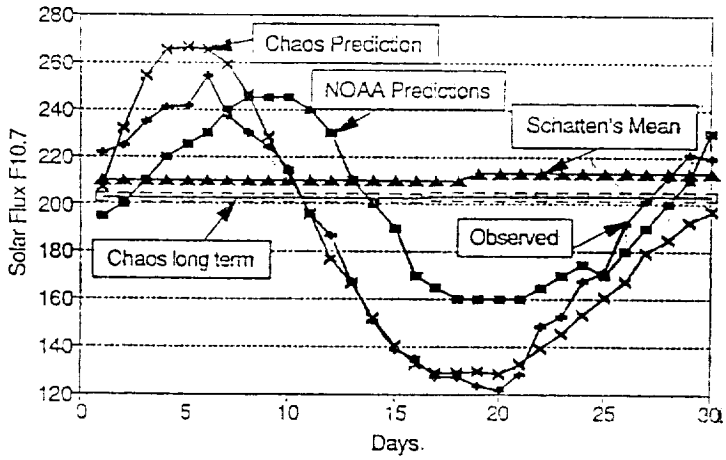

Figure 10. 27-Day Chaos and NOAA Predictions Compared With Observed Solar Flux $F_{10.7}$ From April 13, 1990

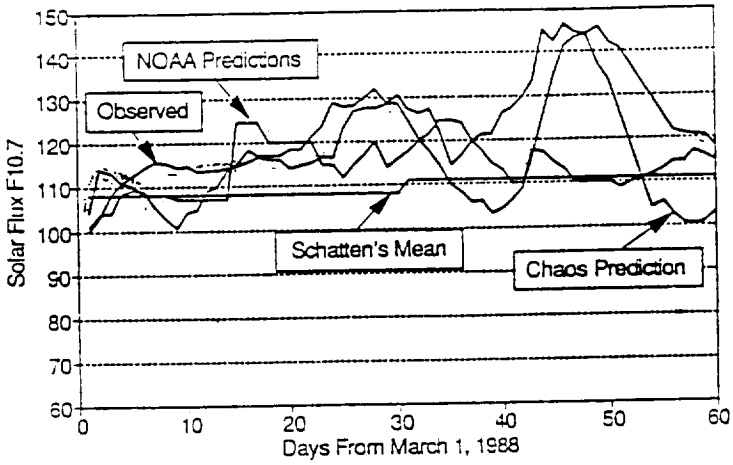

Figure 11. 60-Day Chaos and NOAA Predictions (Best Weekly Updates) Compared With Observed Solar Flux $F_{10.7}$

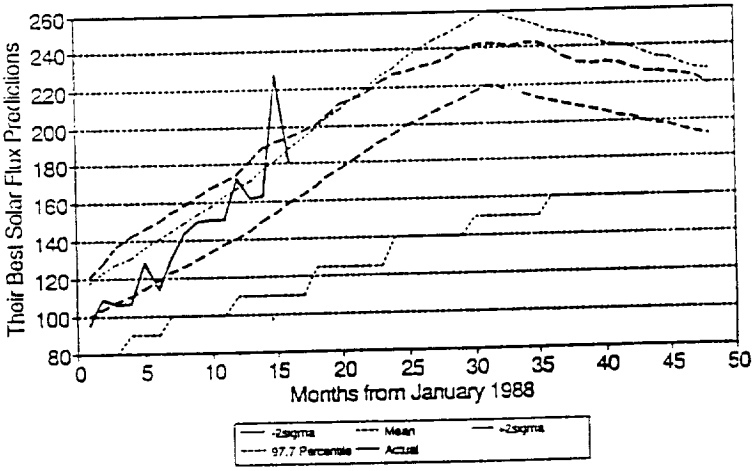

Figure 12. Comparison of MSFC and Schatten Solar Flux $F_{10.7}$ Predictions With Observed $F_{10.7}$

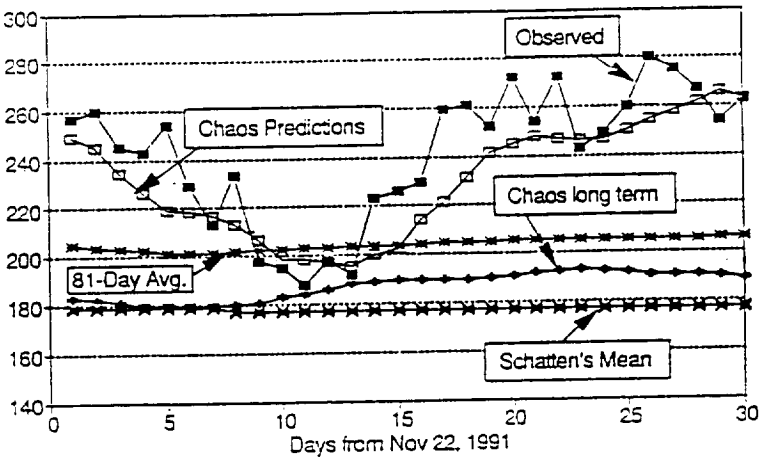

Figure 13. 30-Day Comparison of 81-Day Average of Observed $F_{10.7}$, Schatten's Prediction and Chaos Prediction With Observed Daily $F_{10.7}$

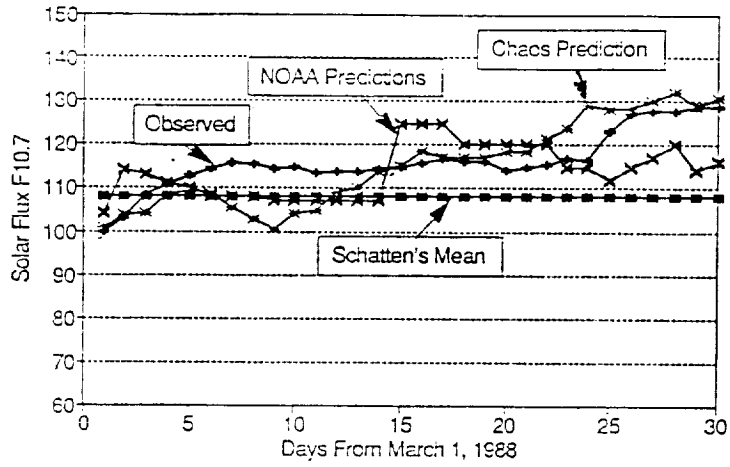

Figure 14. 30-Day Comparison of Schatten's Prediction and Chaos Prediction With Observed Daily $F_{10.7}$

Figure 15 shows chaos predictions for embedding dimensions 3 and 4, the Schatten mean, and $+2\sigma$ predictions. Figure 15 clearly shows that, for long-term forecasting, the chaotic method carries all the inherent structures of Schatten's method. Figure 16 shows that chaos prediction captures the cyclical behavior of solar cycles (the minimum of the cycle is very clear). Figure 17 shows the observed $F_{10.7}$ and its 81-day average, and Figure 18 shows chaos prediction for about 50 months after November 1991 (the time of our analyis). Comparsions of chaotic predictions (Figure 16) with Schatten's predictions show the chaos model to be predicting $F_{10.7}$ even higher than Schatten's $+2\sigma$. Recently, the observed $F_{10.7}$ have in fact been higher than Schatten's $+2\sigma$. As seen in Figure 17, after October the average flux is about 200, as is clear from the first couple of points in Figure 18. It is certainly possible to fine tune the model by adjusting the embedding dimension and the time shift τ. Figure 19 shows predictions for various time shifts τ, with D=3. Figure 20 shows predictions for various time shifts τ, with embedding dimension D=4.

4. CONCLUSIONS

In this paper we presented numerical techniques for constructing nonlinear predictive models to forecast solar flux $F_{10.7}$ directly from its time series. Using this approach, we extracted dynamical invariants of our system

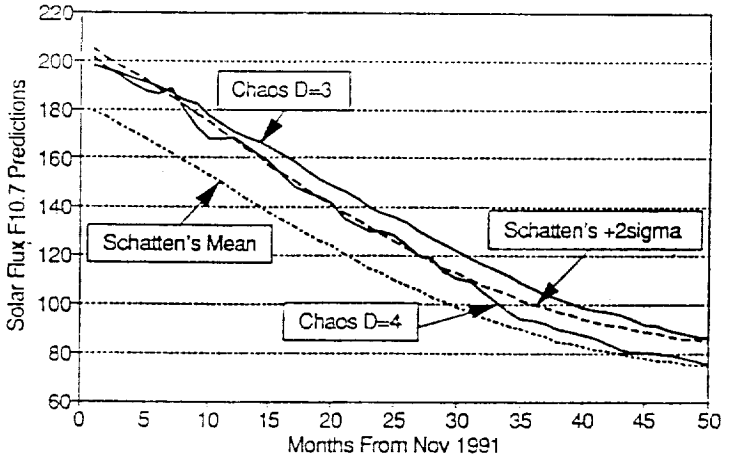

Figure 15. Chaos Long-Term Prediction With Embedding Dimension D=3 and D=4 Compared With Schatten's Mean and Schatten's $+2\sigma$

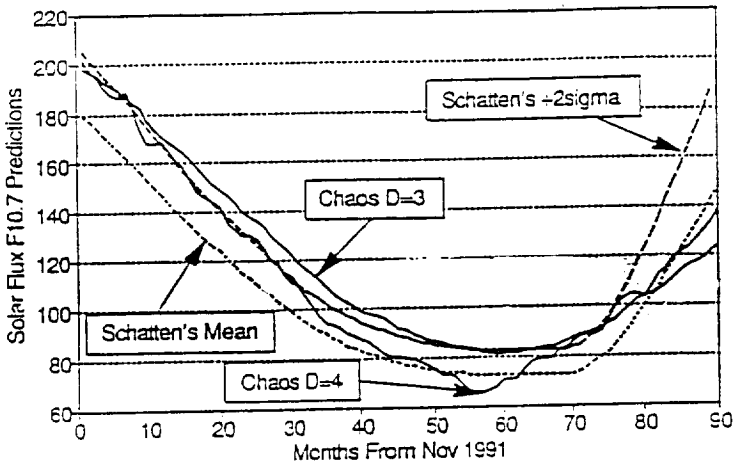

Figure 16. Predictions of Schatten and Chaos Theory for Solar Cycle Minima

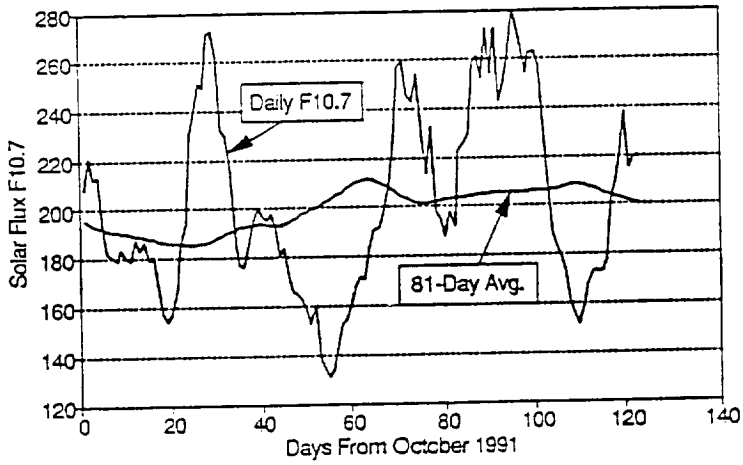

Figure 17. Observed Solar Flux $F_{10.7}$ and Its 81-Day Average, Starting From October 1991

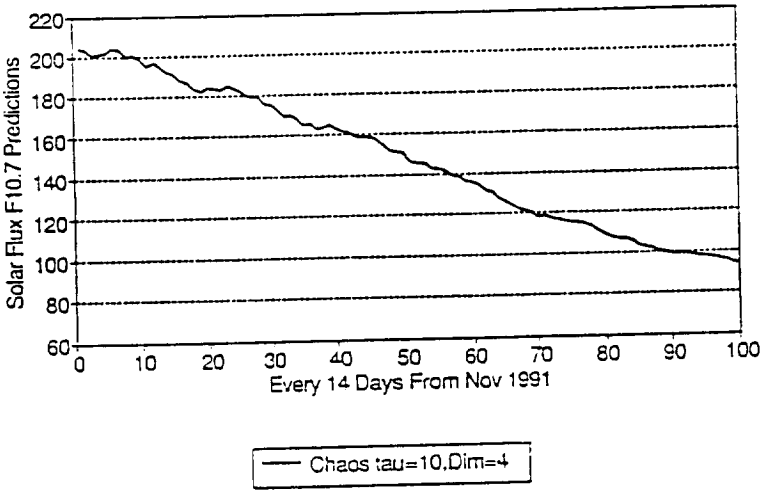

Figure 18. 50-Month Chaos Prediction With Embedding Dimension D=4 and Time Shift τ =10 Days

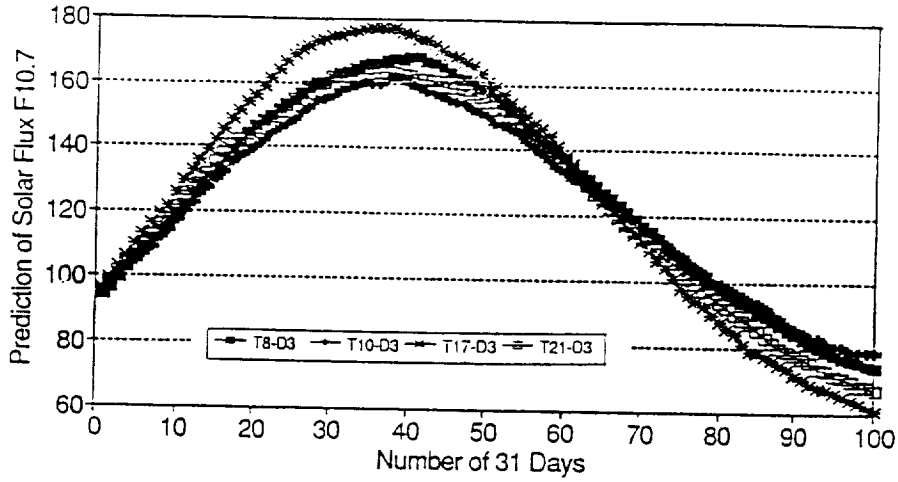

Figure 19. Variability of Predictions as a Function of Change in Time Shift τ. Here Embedding Dimension Is Kept Constant (D=3), and τ Is Varied by 8, 10, 17, and 21 Days

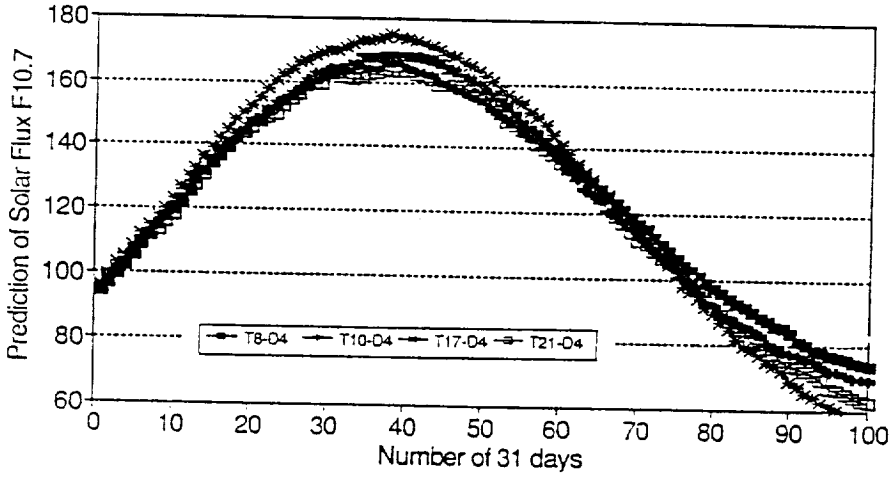

Figure 20. Variability of Predictions as a Function of Change in Time Shift τ. Here Embedding Dimension Is Kept Constant (D=4), and τ Is Varied by 8, 10, 17, and 21 Days

without reference to any underlying solar physics, thereby circumventing the complicated physics and modeling the system directly from data.

Comparison of our prediction of solar flux activity using chaotic dynamics with conventional methods used by Schatten, MSFC, and NOAA demonstrated the validity of our approach to modeling solar activity using nonlinear dynamics. This approach could also be used to model other complicated systems, such as geomagnetic activity and atmospheric density, to name just two.

ACKNOWLEDGMENTS

Thanks to D. Ashrafi, C. Schiff, and J. Kissel for valuable discussions, suggestions, and support. It is also a pleasure to thank K. Schatten for his many suggestions, such as a combined chaos-Schatten model, and C. Grebogi and E. Ott for teaching me the fundamental concepts of chaos (S. A.).

REFERENCES

1. Brandt, C. J., *Introduction to the Solar Wind*, W. H. Freeman and Company, San Francisco, 1990
2. Goddard Space Flight Center, Flight Dynamics Division, *Future Missions Studies: Generalized Model of Sunspots as E-Solitons of Multilevel Turbulence*, S. Ashrafi, in preparation (Computer Sciences Corporation)
3. Goddard Space Flight Center, Flight Dynamics Division, FDD-554-91-004, *Future Missions Studies: Preliminary Comparisons of Solar Flux Models*, S. Ashrafi, prepared by Computer Sciences Corporation, January 1991
4. Goddard Space Flight Center, Flight Dynamics Division, FDD-554-91-006, *Future Missions Studies: Solar Flux Analysis Using Chaos*, S. Ashrafi, prepared by Computer Sciences Corporation, January 1991
5. Evidence of Chaotic Pattern in Solar Flux Through a Reproducible Sequence of Period-Doubling-Type Bifurcations, *Proceedings of Flight Mechanics/Estimation Theory Symposium*, S. Ashrafi and L. Roszman, prepared by Computer Sciences Corporation, May 1991
6. Goddard Space Flight Center, Flight Dynamics Division, 554-FDD-91/112, *Future Missions Studies: Chaotic Solar Flux (Structural Stability, Attractor Dimension, Application of Catastrophe)*, S. Ashrafi, prepared by Computer Sciences Corporation, June 1991
7. Computer Sciences Corporation (under contract to Goddard Space Flight Center, Flight Dynamics Division) *Limits on the Predictability of Solar Flux Time Series*, S. Ashrafi and L. Roszman, June 1991 (submitted for publication in *J. Geophys. Res.*)
8. Goddard Space Flight Center, Flight Dynamics Division, 554-FDD-91/113, *Future Missions Studies: Forecasting Solar Flux Directly From Its Time Series*, S. Ashrafi, prepared by Computer Sciences Corporation, July 1991
9. Goddard Space Flight Center, Flight Dynamics Division, *Future Missions Studies: Existence of a Unique Canonical Transformation to Transform Dynamo Equations to Lorenz Equations*, S. Ashrafi, prepared by Computer Sciences Corporation, unpublished manuscript
10. Goddard Space Flight Center, Flight Dynamics Division, *Future Missions Studies: Intermittency of Dynamo Can Explain Maunder Minimum*, S. Ashrafi, prepared by Computer Sciences Corporation, unpublished manuscript
11. Goddard Space Flight Center, Flight Dynamics Division, 554-FDD-91/125, *Future Missions Studies: Combining Schatten's Solar Activity Prediction Model With a Chaotic Prediction Model*, S. Ashrafi, prepared by Computer Sciences Corporation, November 1991
12. Van Loon, H., and K. Labitzke, Association between the 11-year solar cycle, the QBO, and the atmosphere, Part II, *J. Climate*, 1, 1988
13. Kerr, R. A., Sunspot-weather link is down but not out, *Science*, 248, 1990
14. Bray, J. R., Solar-climate relationships in the post-Pleistocene, *Science*, 171, 1971
15. Walterscheid, R. L., Solar cycle effects on the upper atmosphere: Implications for satellite drag, *J. Spacecraft*, 26, 1989
16. Withbroe, G. L., Solar activity cycle: History and predictions, *J. Spacecraft*, 26, 1989
17. Takens, F., Detecting strange attractors in turbulence, in *Lecture Notes in Mathematics, Vol. 898: Dynamical Systems and Turbulence*, Springer, New York, 1981
18. Packard, N., et al., Geometry From a Time Series, *Phys. Rev. Lett.*, 45, 1980
19. Farmer, J., and J. Sidorowich, Predicting chaotic time series, *Phys. Rev. Letts.*, 59, 1987
20. Abarbanel, H., et al., Lyapunov exponents in chaotic systems, *Rev. Modern Phys. Letts.* [B], (in press)
21. Bentley, J. H., Multidimensional binary search trees in data base applications, *IEEE Transactions on Software Engineering*, 5 (4), 1979